Title
In vivo and in vitro Models of Demyelinating Diseases

Journal
Intervirology, 18(3)

ISSN
0300-5526

Authors
Massalski, Andrew
Coulter-Mackie, Marion
Knobler, Robert L
et al.

Publication Date
1982

DOI
10.1159/000149316

Peer reviewed

Intervirology *18:* 135–146 (1982)

In vivo and in vitro Models of Demyelinating Diseases

V. Comparison of the Assembly of Mouse Hepatitis Virus, Strain JHM, in Two Murine Cell Lines

Andrew Massalski[a], *Marion Coulter-Mackie*[a], *Robert L. Knobler*[b], *Michael J. Buchmeier*[b], *Samuel Dales*[a]

[a]Cytobiology Group, Department of Microbiology and Immunology, University of Western Ontario, London, Ont., Canada;
[b]Department of Immunopathology, Scripps Clinic and Research Foundation, La Jolla, Calif., USA

Key Words. Demyelinating diseases · Mouse hepatitis virus · Coronaviruses

Summary. The developmental sequence of a neurotropic strain (JHM) of mouse hepatitis virus was examined by transmission electron microscopy and immunocytology. The nucleoprotein core of this coronavirus, which contains RNA of positive polarity and is helical in configuration, becomes incorporated into enveloped particles in the same manner as the nucleocapsids of the orthomyxo- and paramyxoviruses. However, JHM virus is assembled intracellularly by budding at surfaces of smooth membranous vacuoles. A comparison of JHM virus replication in L2 and 17Cl-1 cell lines revealed that L2 cells undergo more rapid cytopathology and cease virus production much sooner than 17Cl-1 cells. In L2 cells the accumulation of core material appears to continue after the abrupt cessation of virus assembly. This is evident by the massive cytoplasmic accumulation of structures resembling nucleocapsids, which react with hybridoma antibody to the nucleocapsid antigen as demonstrated by the immunoperoxidase procedure. The current findings are consistent with our previously published demonstration, using cells of neural and other deviation, of the fundamental role of the host cell type in regulating the replication and expression of coronaviruses.

Coronaviruses have been characterized as a separate group [1] predominantly based on the morphology of their unique, massive peplomers and single-stranded +RNA genome [2]. Electron microscopic studies on different members of this group revealed that assembly occurs in the cytoplasm, where progeny are formed by a budding process from membranes of the endoplasmic reticulum and/or cytoplasmic vacuoles [3]. The budding process has been described in some detail in the

Address inquiries to: Dr. Samuel Dales, Cytobiology Group, Department of Microbiology and Immunology, University of Western Ontario, London, Ont. N6A 5C1 (Canada)

Received: December 8, 1981
Revised: February 24, 1982

case of avian infectious bronchitis virus, the human agent (229E [4]), and other isolates [5–14]. Although most data favor budding as the assembly mechanism, some reservations have been made about the significance of this process [15, 16]. During replication of the neurotropic strain JHM of mouse hepatitis virus in oligodendrocytes, within the central nervous system of rats manifesting chronic demyelinating disease, there are evident few virions and large cytoplasmic inclusions consisting of elements resembling virus cores [17]. By contrast, during highly productive cycles of JHM virus replication in the 17Cl-1 cell line, such inclusions are absent [18]. The present investigation was undertaken to ascertain whether deficient assembly of virions and accumulation of nucleocapsids are interrelated phenomena.

Materials and Methods

Cells and Viruses

Mouse 17Cl-1 cells of the 17th passage are derivative of 3T3 BALB/c cells and were kindly provided by Dr. *L.S. Sturman* (Division of Laboratories and Research, New York State Department of Health, Albany, N.Y.). The derivation and methods for propagating, in suspension or as monolayers, murine L2 cells have been described previously [19]. These lines are routinely maintained in Eagle's MEM supplemented with 10% heat-inactivated fetal bovine serum (Microbiological Associates), sodium bicarbonate (2 g/l), penicillin (100 U/ml) and streptomycin (100 mg/l) in a humidified atmosphere with 5% CO_2. The JHM strain of murine coronavirus was obtained from the American Type Culture Collection (Rockville, Md.).

Growth of JHM Virus and Infection of Cells for Electron Microscopy

Both L2 and 17Cl-1 cells were grown to monolayer in 20-mm plastic tissue culture dishes and infected with JHM virus at a multiplicity of 0.004–0.2 PFU/cell. After 1 h adsorption at 32.5°, cultures were washed with phosphate-buffered saline, overlaid with 2 ml MEM, and incubated at 32.5° for 24 or 48 h prior to sampling. A range of multiplicities was employed to obtain samples representing various stages of infection at 24 and 48 h, the two times chosen for sampling.

Virus Assays

The quantity of infectious JHM virus was ascertained by plaque assay on monolayers of L2 cells as described [19]. The overlay medium contained 0.7% methylcellulose, and incubation for optimum plaque development was for about 48 h at 37°.

Electron Microscopy

Cell monolayers in which syncytia formation was evident were fixed in situ by flooding with 2% glutaraldehyde in 0.05 *M* phosphate buffer at pH 7.2 and post-fixed with 1% OsO_4 according to our previously described method [20]. Following washing and dehydration in ethanol series, the cells were infiltrated with a 1:1 mixture of absolute ethanol and Epon 812. The monolayers were finally covered with an approximately 2–3 mm thick layer of Epon 812 and were polymerized at 60° for 24 h. Small fragments of the hardened disks were cut out and mounted in orientations which permitted the monolayer to be sectioned both horizontally and vertically. Unsupported 200-mesh grids were used to collect sections, which were subsequently double-stained for 4 min with 5% uranyl acetate in 50% ethanol, followed by 3 min with lead citrate solution [21]. The specimens were examined in a Philips EM300 at an accelerating voltage of 60 or 80 kV.

Immunocytochemistry

Monolayers containing syncytia were fixed 18 h postinfection in 2% paraformaldehyde. The washing and immunoperoxidase staining method were essentially as described [22]. The hybridoma antibody against the nucleocapsid antigen, designated 46B.2 [23], was used at a 1:100 dilution.

Results and Discussion

Comparison of JHM Virus Replication in L2 and 17Cl-1 Cells

The differences in rates of cytopathology and virus development evident in the light microscope suggested that it would be informative to compare formation of infectious

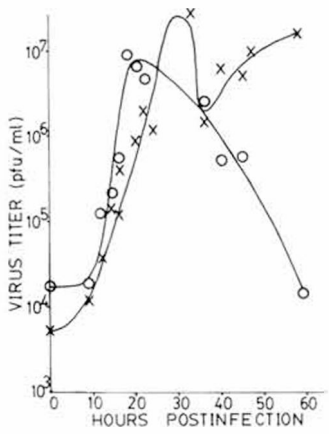

Fig. 1. Comparison of JHM virus replication in 17Cl-1 (×) and L2 (○) cells. Confluent monolayers in 30-mm Petri dishes were inoculated with 0.1 PFU/cell and incubated throughout at 32.5°. At regular intervals, cultures were examined microscopically and sampled for estimation of total virus (i.e., extracellular plus cell-associated) as follows. Attached cells were scraped and suspended in 2 ml of the incubation medium. The material was rapidly frozen-thawed three times and the lysates were suitably diluted for plaque assays.

progeny in the two host cells. For this purpose, monolayers were inoculated at a multiplicity of 0.1 PFU/cell, consistent with procedures employed to follow the infectious process by electron microscopy. It should be pointed out that inoculation with higher multiplicities (>3 PFU/cell), required for synchronizing the virus growth cycle, caused uncontrollable CPE, including premature detachment of cells from the substrate, so as to mitigate against studies of assembly of the type undertaken here.

A comparison of the growth cycles of JHM virus in the two host cells (fig. 1) demonstrated clearly that in L2 cells peak titers were reached more rapidly, within 20 h postinoculation, and thereafter an abrupt fall in virus production occurred. By contrast, in 17Cl-1 cells, virus production reached somewhat higher maximum levels by 30 h, and then virus production continued at an elevated rate for a much longer period than in L2 cells, beyond the cessation of the experiment 60 h after inoculation. An apparent trough in JHM virus titer, evident in figure 1 at about 40 h, was followed by a second rise in PFUs, which was most likely due to an additional wave of infection. In this connection it should be mentioned that after inoculation with 0.1 PFU/cell, 17Cl-1 cells undergo minor syncytia formation in foci scattered throughout the monolayer. The individual polykaryocytes did not appear to coalesce into progressively growing syncytia, unlike the situation prevailing in the L2 cell cultures. Furthermore, infected 17Cl-1 cells remained attached to the substrate for several (3–4) days, whereas the massive L2 cell syncytia became detached within 24 h and lysed in less than 48 h.

Electron Microscopy of Virus Development

To facilitate sampling for examination of virus development by transmission electron microscopy, monolayers of 17Cl-1 and L2 cells were infected with JHM virus at multiplicities sufficiently low to initiate progressive syncytiogenesis, as described previously [19]. With 17Cl-1 cells, the small syncytia scattered throughout the monolayers became evident initially within 24 h postinfection and increased to a limited extent by 48 h. In contrast to the cytopathology associated with JHM virus infection of 17Cl-1 cells, the progressive development of syncytia in monolayers of L2 cells, inoculated at about the same low multiplicity (0.004–0.1 PFU/cell), was much more rapid and extensive [19], involving practically the whole monolayer within 24–36 h. For this reason, cultures of this host cell type were sampled for electron microscopy within 24 h postinfection.

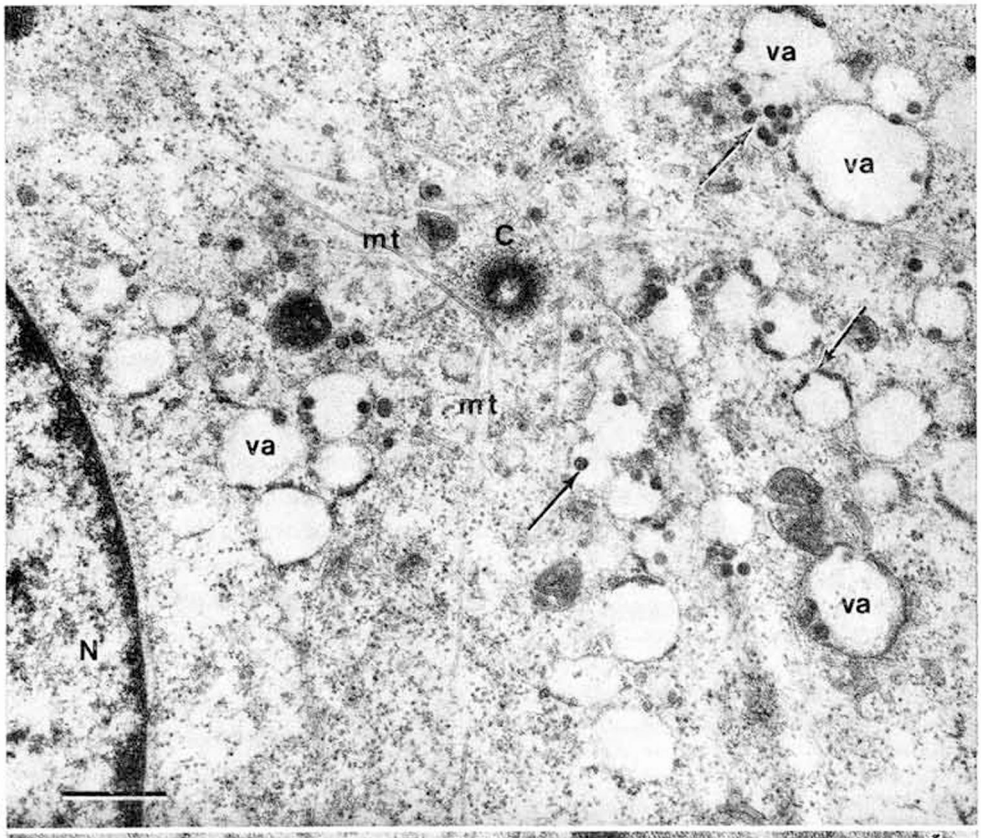

2

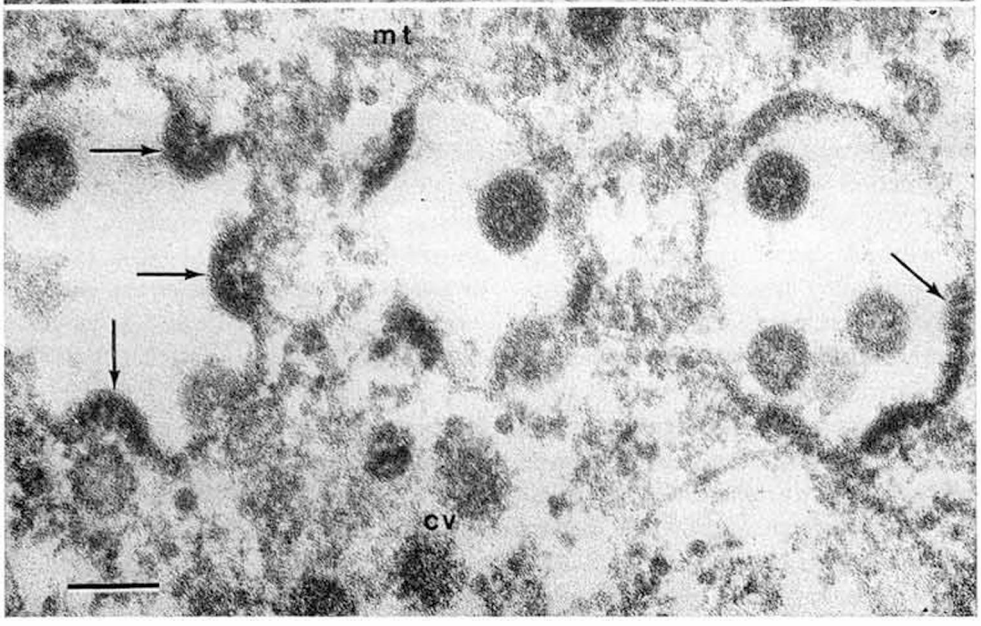

3

4

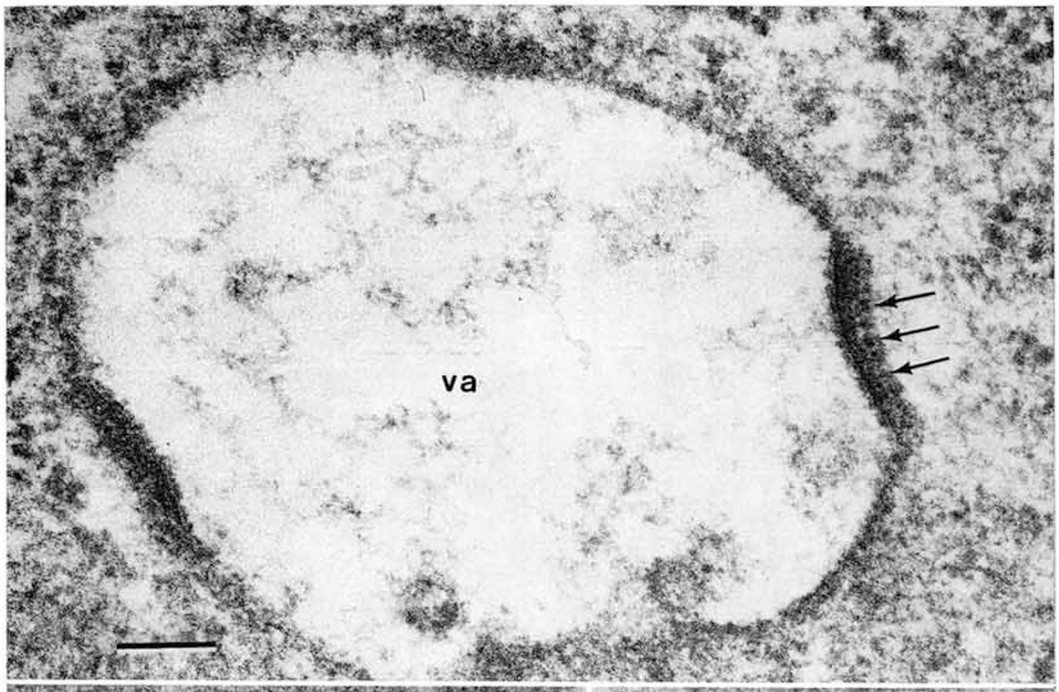

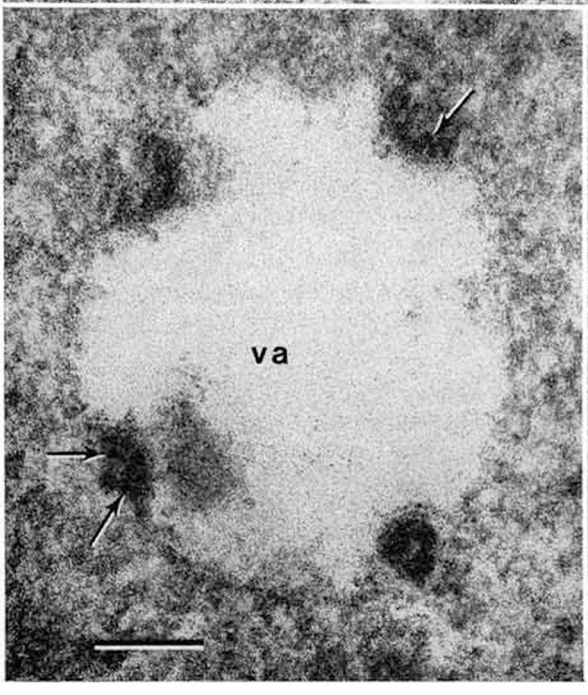

5

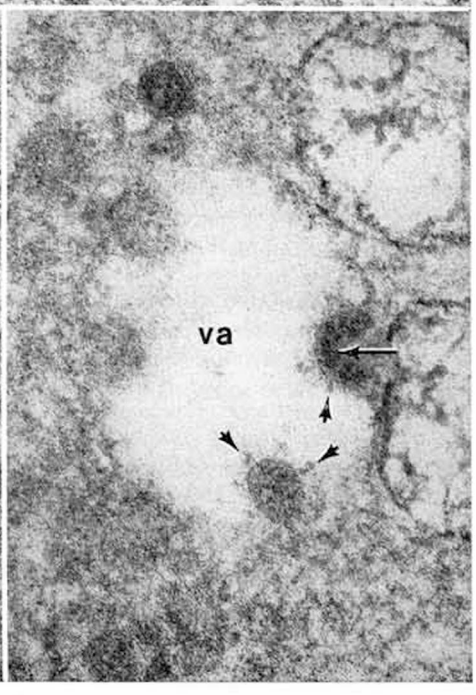

6

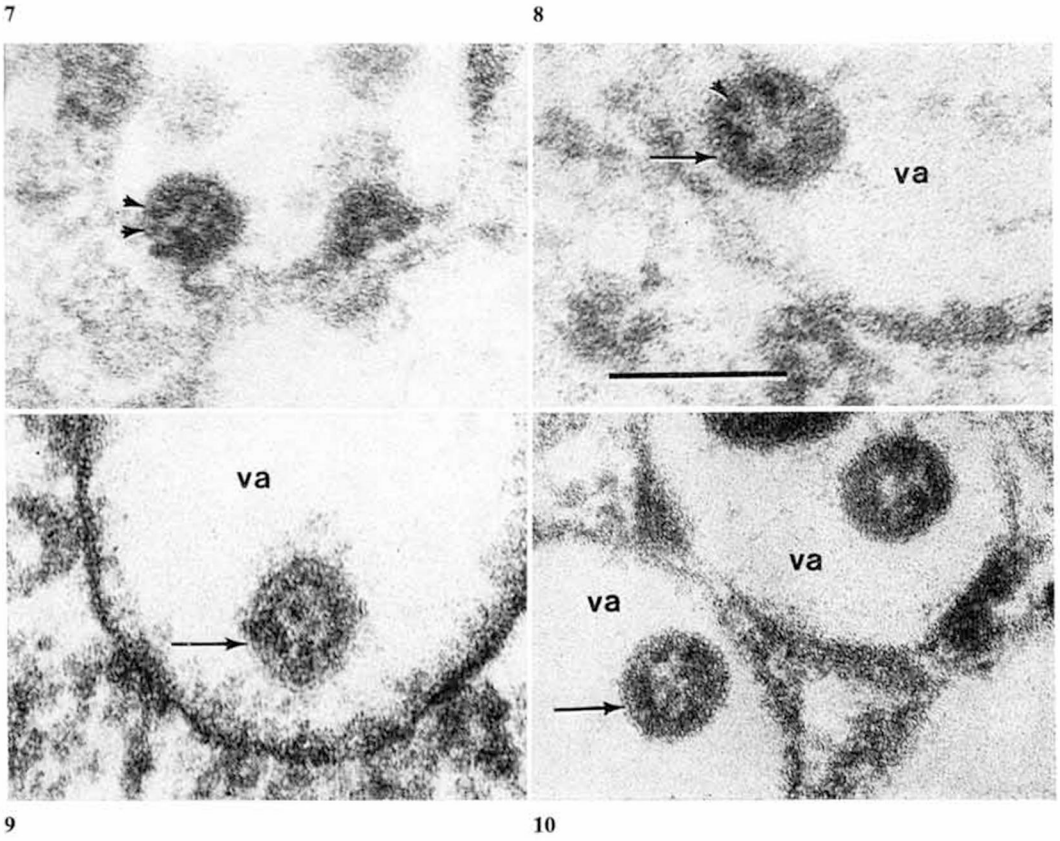

Fig. 2–15. Selected areas of sections of infected 17Cl-1 (fig. 2, 3, 7–12) and L2 (fig. 4–6, 13, 14) cells, sampled respectively, 48 and 24 h after inoculation. Monolayers were preserved in situ to illustrate assembly and intracellular distribution of virus progeny. (Bars in figures 2 and 13, 0.5 μm; all others, 0.1 μm).

Fig. 2. At a lower magnification, note presence of cytoplasmic vacuoles (va) containing budding or free virus particles (arrows). C = Centriole; mt = microtubules; N = nucleus. × 31,000.

Fig. 3. An example at higher resolution reveals stages of virus assembly at the membranes of vacuoles (arrows). mt = Microtubule; cv = coated vesicle. × 138,000.

Fig. 4. Early phase of budding. The symmetrically organized internal component (arrows) is clearly evident subjacent to the assembling envelope. va = Vacuoles. × 130,000.

Fig. 5, 6. Advanced stages in virus assembly. The internal cores are indicated by arrows. Peplomers, evident on surfaces of virions inside vacuoles, are indicated by arrowheads. va = Vacuoles. × 145,000.

Fig. 7–10. Selected areas at high resolution demonstrating virus budding at membranes of vacuoles. The virus envelope, either in continuity with the vacuole membrane (fig. 7) or enclosing virions (fig. 8–10), is indicated by arrows. The nucleocapsids, indicated by arrowheads, are evident as tubular structures in either the longitudinal aspect or in cross section (fig. 7, 8) during the formative stages and in completed virions. Peplomers are also evident in the particle in figure 9. va = Vacuole. Figure 8, × 240,000; all others, × 200,000.

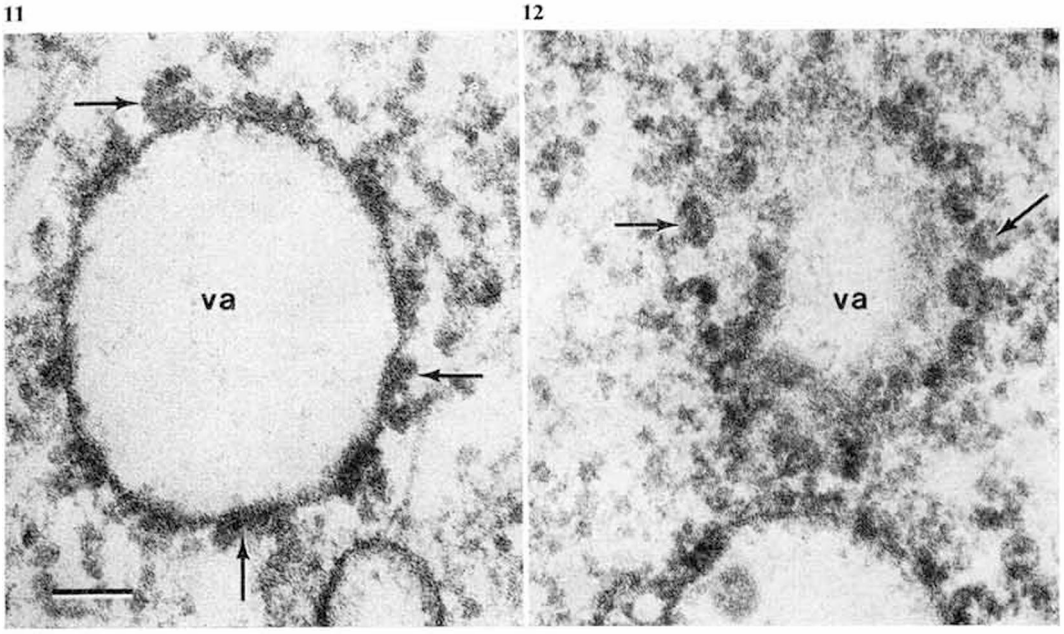

Fig. 11, 12. Vacuoles in transverse (fig. 11) and tangential (fig. 12) sections surrounded by dense material (arrows) presumed to be the viral nucleoprotein component of cores. Note the similarity in structure of this material and the internal component of virions, evident at vacuoles (va) where budding was occurring. × 112,000.

To preserve as faithfully as possible the structural relationship between sites of virus development and related cellular organelles, as they occurred in the living state, fixation and embedding of attached cells were carried out in situ. This procedure facilitated a precise localization and selection of areas in the monolayer where syncytiogenesis was evident by light microscopy.

Examination of horizontally sectioned syncytia revealed the presence of numerous vacuoles, ranging in diameter from 150 to 160 nm (fig. 2). Absence of ribosomes on the cytoplasmic face of the vacuole membranes implies that these structures are derived from smooth endoplasmic reticulum (SER). Their random distribution, as ascertained by both vertical and horizontal sections, implies that they occur throughout the cytoplasm. Occurrence of circular, rather than flattened, profiles of the sectioned vacuoles indicates that the SER becomes distended following infection. Virus assembly is confined to these vacuoles (fig. 2–10) and has not been observed at the plasma membrane or any other cellular surface. This is in agreement with other studies of the coronaviruses [2, 24], but at variance with sites of assembly of enveloped viruses from the orthomyxo-, paramyxo-, and rhabdovirus groups [25–27].

An interpretation of the dynamic events during JHM virus assembly in polykaryocytes was based upon a series of images, ordered into a developmental sequence (fig. 3–10). The

most rudimentary stage was identified by the presence of a short segment of dense material subjacent to the vacuolar membrane (fig. 3, 4). An associated unit membrane was clearly evident on the external surface and is presumed to represent the viral envelope covered by the peplomers (fig. 6, 9). Elongated structures, which in some images appeared to be tubular in nature, were organized on the cytoplasmic side of the modified vacuolar surface (fig. 3–6). In the more advanced stages of budding, the virus envelope surrounded the elongated, internal component to a varying degree (fig. 3, 7–10). In favorable orientations the tubular nature of the internal component could be discerned (fig. 4–8).

The JHM virus cores are highly reminiscent of the nucleoprotein helix of influenza virus [28]. The external diameter of the coronavirus tubules is on the average 9.5 nm, ranging from 8.5 to 10.0 nm. These dimensions correspond to measurements made on the extruded coronavirus helical component, evident by negative staining [29, 30], and on a dense internal thread present within thinly sectioned, infectious avian bronchitis virus [28]. An internal component of greater diameter has been recorded in one study [31]. Our measurements also correspond to the diameter of the influenza virus nucleoprotein, which has a diameter of either 6–9 nm in sectioned virions [28] or 10–15 nm in whole mount preparations [25, 26]. By contrast, the diameter of the helical nucleocapsid of the paramyxoviruses, measuring 15–19 nm [24, 32, 33], is about double the width of the coronavirus cores. According to another recent interpretation, the coronavirus nucleocapsid structure is described as a circular, dense, inner component, about 60 nm in diameter [7]. Our new evidence, coupled with information obtained on disrupted negatively stained 229E virions [29, 31] and on another representative of the group [30], indicate that the architecture of the coronaviruses simulates that of the orthomyxo- and paramyxoviruses, although the coronaviruses, unlike the other two groups, possess a single-stranded RNA genome of the + sense. From this observation it may be concluded that polarity of the RNA genome and helical conformation of the nucleoprotein are not necessarily interrelated.

With 17Cl-1 cell syncytia, occasionally large vacuoles were evident, surrounded by numerous dense, fibrillar structures of the same appearance as virus cores (fig. 11, 12). Unlike the more frequently observed process of budding, such core-like fibers apparently were not being wrapped inside envelopes.

The electron microscopic evidence showed that during extensive and rapid syncytiogenesis, elicited by JHM virus in L2 cells, there were fewer formative budding or completed intravacuolar virions than found in syncytia of 17Cl-1 cells. On the other hand, extensive accumulations of aggregates consisting of a core-like component were frequently present in the cytoplasm of L2 cell polykaryocytes (fig. 13). At higher resolution (fig. 14), these aggregates consisted of elements possessing the same structure as virion cores (fig. 3–10) and the vacuole-associated fibers evident in 17Cl-1 cells (fig. 11, 12). This material of the inclusions was demonstrated, by the immunoperoxidase procedure, to contain the nucleocapsid antigen of mouse hepatitis virus (fig. 15), corroborating the morphological evidence about the nature of this material.

Masses of nucleocapsids accumulate in syncytia induced by infection with other enveloped agents like the paramyxoviruses, as in the case of measles virus infection of the BHMK cell line [34] and infection by simian virus 5 of BHK21 hamster cells [32]. In vivo, chronic progressive infection of the rat central nervous

13

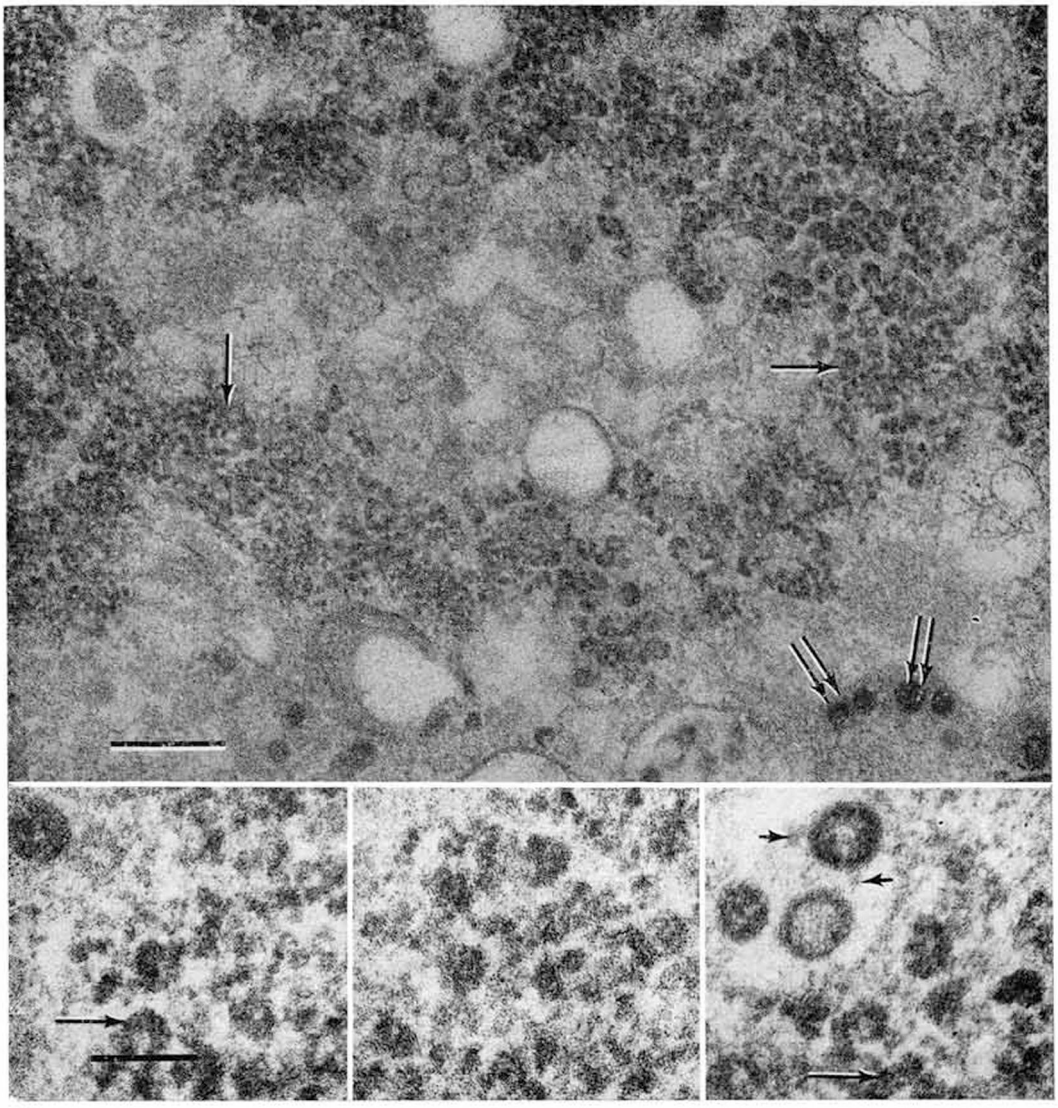

14

Fig. 13. Selected area illustrates, at lower magnification, the extensive cytoplasmic accumulations of dense fibrous material (single arrows). Intravacuolar virions (double arrows) are also evident in this example. × 30,000.

Fig. 14. Examples at high resolution illustrate the morphology of the components within the aggregates. Arrows point to individual elements which are similar in structure to fibers within virions (fig. 4–10) or on the cytoplasmic face of vacuoles (fig. 11, 12). Arrowheads point towards peplomers on a virion, within a vacuole. × 130,000.

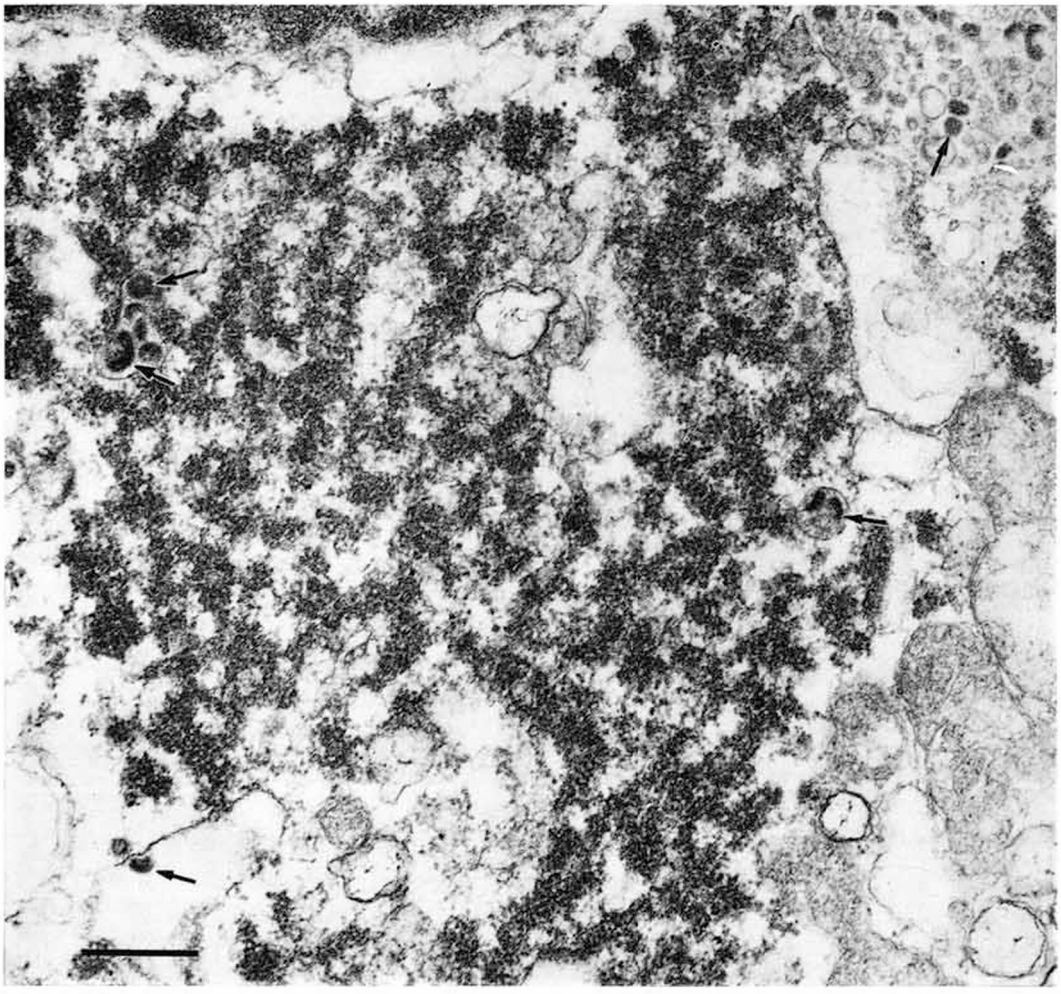

Fig. 15. Staining of nucleocapsid antigen by immunoperoxidase, in the cytoplasm of an L2 polykaryocyte, preserved 18 h after inoculation of the monolayer. Electron-dense deposits of the reaction product occur within virions (arrows), and material constituting the massive inclusion appears at the center of the field. × 31,000.

system, which may involve exclusively the oligodendrocytes, also leads to development of extensive cytoplasmic aggregates like those described here [17].

In conclusion, the combined data from electron microscopy and growth cycles clearly indicate that replication of JHM virus in the 17Cl-1 cell line occurs in a more orderly and efficient manner for prolonged periods, although assembly of infectious particles may be initiated more gradually than in L2 cells. On the other hand, rapid syncytiogenesis and cell killing caused in L2 cells by JHM virus might underlie the reduced efficiency in the

wrapping and budding assembly sequence, resulting in accumulation of excessive nucleocapsid cores within the cytoplasm. The current observations once again emphasize the importance, evident from our previous studies [19] with cells of neural and other origin, of the host in regulating the coronavirus infectious process, including cytopathology.

Acknowledgments

This work was supported by grants from the Multiple Sclerosis Society and Medical Research Council of Canada to S. D. and by USPHS grant NS12428. R. L. K. is a Fellow of the National Multiple Sclerosis Society.

References

1 Tyrrell, D.A.J.; Almeida, J.D.; Cunningham, C.H.; Dowdle, W.R.; Hofstad, M.S.; McIntosh, K.; Tajima, M.; Zakstelskaya, L.Y.; Easterday, B.C.; Kapikian, A.; Bingham, R.W.: Coronaviridae. Intervirology *5*: 76–82 (1975).

2 Robb, J.A.; Bond, C.W.: Coronaviridae; in Fraenkel-Conrat, Wagner, Comprehensive virology, vol. 14, pp. 193–247 (Plenum, New York 1979).

3 David-Ferreira, J.F.; Manaker, R.A.: An electron microscope study of the development of a mouse hepatitis virus in tissue culture cells. J. Cell Biol. *24*: 57–78 (1965).

4 Becker, W.B.; McIntosh, K.; Dees, J.H.; Chanock, R.M.: Morphogenesis of avian infectious bronchitis virus and a related human virus (strain 229E). J. Virol. *1*: 1019–1027 (1967).

5 Chasey, D.; Alexander, D.J.: Morphogenesis of avian infectious bronchitis virus in primary chick kidney cells. Archs. Virol. *52*: 101–111 (1976).

6 Cunningham, C.H.; Spring, M.P.; Nazerian, K.: Replication of avian infectious bronchitis virus in African green monkey kidney cell line VERO. J. gen. Virol. *16*: 423–427 (1972).

7 Fleury, H.J.A.; Sheppard, R.D.; Bornstein, M.B.; Raine, C.S.: Further ultrastructural observations of virus morphogenesis and myelin pathology in JHM virus encephalomyelitis. Neuropath. appl. Neurobiol. *6*: 165–179 (1980).

8 Nazerian, K.; Cunningham, C.H.: Morphogenesis of avian infectious bronchitis virus in chicken embryo fibroblasts. J. gen. Virol. *3*: 469–470 (1968).

9 Oshiro, L.S.; Schieble, J.H.; Lennette, E.H.: Electron microscopic studies of coronavirus. J. gen. Virol. *12*: 161–168 (1971).

10 Robb, J.A.; Bond, C.W.: Pathogenic murine coronaviruses. I. Characterization of biological behavior *in vitro* and virus-specific intracellular RNA of strongly neurotropic JHMV and weakly neurotropic A59V viruses. Virology *94*: 352–370 (1979).

11 Robb, J.A.; Bond, C.W.; Leibowitz, J.L.: Pathogenic murine coronaviruses. III. Biological and biochemical characterization of temperature-sensitive mutants of JHMV. Virology *94*: 385–399 (1979).

12 Ruebner, B.H.; Hirano, T.; Slusser, R.J.: Electron microscopy of the hepatocellular and Kupffer cell lesions of mouse hepatitis with particular reference to the effect of cortisone. Am. J. Path. *51*: 163–190 (1967).

13 Watanabe, K.: Electron microscopic studies of experimental viral hepatitis in mice. I. Virus particles and their relationship to hepatocytes and Kupffer cells. J. Electron Microsc. *18*: 158–172 (1969).

14 Witte, K.H.; Tajima, M.; Easterday, B.C.: Morphologic characteristics and nucleic acid type of transmissible gastroenteritis virus of pigs. Arch. ges. Virusforsch. *23*: 53–70 (1968).

15 Hamre, D.; Kindig, D.A.; Mann, J.: Growth and intracellular development of a new respiratory virus. J. Virol. *1*: 810–816 (1967).

16 Uppal, P.K.; Chu, H.P.: An electron microscope study of the trachea of the fowl infected with avian infectious bronchitis virus. J. med. Microbiol. *3*: 643–647 (1970).

17 Sorensen, O.; Percy, D.; Dales, S.: *In vivo* and *in vitro* models of demyelinating disease. III. JHM virus infection of rats. Archs Neurol., Chicago *37*: 478–484 (1980).

18 Massalski, A.; Dales, S.: Assembly of mouse hepatitis virus strain JHM; in ter Meulen, Siddell, Wege, Biochemistry and biology of coronaviruses. Adv. exp. Biol. Med., vol. 42, pp. 111–118 (Plenum, New York 1981).

19 Lucas, A.; Flintoff, W.; Anderson, R.; Percy, D.; Coulter, M.; Dales, S.: In vivo and in vitro models of demyelinating diseases: tropism of the JHM

strain of murine hepatitis virus for cells of glial origin. Cell *12:* 553–560 (1977).

20 Dales, S.; Hanafusa, H.: Penetration and intracellular release of the genomes of avian RNA tumor viruses. Virology *50:* 440–458 (1972).

21 Reynolds, E.S.: The use of lead citrate at high pH as an electron-opaque stain in electron microscopy. J. Cell Biol. *17:* 208–211 (1963).

22 Knobler, R.L.; Dubois-Dalcq, M.; Haspel, M.V.; Claysmith, A.P.; Lampert, P.W.; Oldstone, M.B.A.: Selective localization of wild type and mutant mouse hepatitis virus (JHM strain) antigens in CNS tissue by fluorescence, light and electron microscopy. J. Neuroimmunol. *1:* 81–92 (1981).

23 Collins, A.R.; Knobler, R.L.; Powell, H.; Buchmeier, M.J.: Monoclonal antibodies to murine hepatitis virus-4 (strain JHM) define the viral glycoprotein responsible for attachment and cell-cell fusion (submitted for publication).

24 Choppin, P.W.; Stoeckenius, W.: The morphology of SV5 virus. Virology *23:* 195–202 (1964).

25 Compans, R.W.; Content, J.; Duesberg, P.H.: Structure of the ribonucleoprotein of influenza virus. J. Virol. *10:* 795–800 (1972).

26 Pons, M.W.; Schulze, I.T.; Hirst, G.K.: Isolation and characterization of the ribonucleoprotein of influenza virus. Virology *39:* 250–259 (1969).

27 Wagner, R.R.: Reproduction of rhabdoviruses; in Fraenkel-Conrat, Wagner, Comprehensive virology, vol. 4, pp. 1–93 (Plenum, New York 1975).

28 Apostolov, K.; Flewett, T.H.; Kendal, A.P.: Morphology of influenza A, B, C and infectious bronchitis virus (IBV) virions and their replication; in Barry, Mahy, The biology of large RNA viruses, pp. 3–26 (Academic Press, New York 1970).

29 Kennedy, D.A.; Johnson-Lussenburg, C.M.: Isolation and morphology of the internal component of human coronavirus, strain 229E. Intervirology *6:* 197–206 (1975/76).

30 Pocock, D.H.; Garwes, D.J.: The polypeptides of haemagglutinating encephalomyelitis virus and isolated subviral particles. J. gen. Virol. *37:* 487–499 (1977).

31 Macnaughton, M.R.; Davies, H.A.; Nermut, M.V.: Ribonucleoprotein-like structures from coronavirus particles. J. gen. Virol. *39:* 545–549 (1978).

32 Compans, R.W.; Holmes, K.V.; Dales, S.; Choppin, P.W.: An electron microscopic study of moderate and virulent virus-cell interactions of the parainfluenza virus SV5. Virology *30:* 411–426 (1966).

33 Norrby, E.C.J.; Magnusson, P.: Some morphological characteristics of the internal component of measles virus. Arch. ges. Virusforsch. *17:* 443–447 (1965).

34 Coulter-Mackie, M.B.; Bradbury, W.C.; Dales, S.; Flintoff, W.F.; Morris, V.L.: *In vivo* and *in vitro* models of demyelinating diseases. IV. Isolation of Hallé measles virus-specific RNA from BGMK cells and preparation of complementary DNA. Virology *102:* 327–338 (1980).